Modeling three-dimensional bait ball collective motion

Danshi Liu, Yanhong Liang, and Jian Deng*
Department of Mechanics, Zhejiang University, Hangzhou 310027, People's Republic of China

Wei Zhang
Science and Technology on Water Jet Propulsion Laboratory, Marine Design and Research Institute of China, Shanghai 200011, People's Republic of China

(Received 7 July 2022; revised 4 December 2022; accepted 6 January 2023; published 18 January 2023)

Collective motion of animal groups such as fish schools and bird flocks in three-dimensional (3D) space are modeled by considering a topological (Voronoi) neighborhood. The tridimensionality of the group is quantified. Apart from the patterns of swarming, schooling, and milling, we identify a 3D bait ball around the phase transition boundary. More significantly, we find that by considering a blind angle in this topology based model, an individual interacts statistically with six to seven neighbors, consistent precisely with the previous field observations of the starling flocks. This model could be expected to enable more insightful investigation on realistic collective motion of shoals or flocks.

DOI: 10.1103/PhysRevE.107.014606

I. INTRODUCTION

Collective motion is a widespread phenomenon in biological systems, which has been attracting increasing interest from different scientific communities, spanning from biologists and neuroscientists to physicists and mathematicians [1–4]. From a biologist's point of view, the characteristics of biological systems are not all the same, and even single individuals do not always respond the same way to stimuli. However, physicists have been trying to build a single unified model of collective behavior in biology, which is clearly not possible. We must acknowledge that the goal of physical model is to explicate general principles of how global properties can arise from local interactions, and perhaps to constrain what kinds of properties are possible. In this context, in 1995 Vicsek *et al.* [5] proposed a simple self-propelled particles (SPP) model, which considers identical particles moving at a constant velocity and interacting locally by trying to align their neighbors [6,7]. Built upon a constant swimming speed and an autocorrelation of the angular speed (turning angle per unit time), a persistent turning walker (PTW) model was proposed [8,9], which was then further developed by considering an additional frontal preference in the stimulus/response function to account for the angular weighting of interactions (a more intelligent sensory strategy). Multistability and intermittence between schooling and milling were observed [10–12].

The most critical step in the aforementioned models is to determine the interacting range, or the neighbors an individual agent tends to align with. As previously reviewed [13], there have been three main definitions of neighborhood on which the interactions are calculated. First, the metric neighborhood, where all individuals within a specified distance are taken into account [14–16]. Second, the topological neighborhood that remains invariant with respect to density changes, which can be achieved either by considering a fixed number of neighbors according to their proximity (K nearest neighbors) [17] or by using the first shell of a Voronoi tessellation [18–20]. The third approach is derived from visual processing considerations, corresponding to a dynamical selection of the neighborhood based on selective attention to motion [21,22]. Based on 22 flocking events of the starling flocks, it was found that each bird interacts approximately with 7 ± 1.5 closest neighbors [23], irrespective of the density of the flock. However, we should also note that in fish schools, experimental studies suggest that each individual interacts with a smaller number of influential neighbors [24–28].

Natural collective motions are generally run in 3D space, such as fish school whirling and starling flocking. Though the original Vicsek model was confined in 2D space, its extension to 3D space appears to be straightforward [29–33]. Since the variations of the Vicsek model usually consider metric neighborhood with periodic conditions, their 3D simulations found similar behaviors in terms of disorder-order transition as that in two dimensions, such as the occurrence of density waves [30], and the aggregation of particles (phase separation) [31,32]. Dividing a sphere centered at an individual into zones of repulsion, orientation, and attraction, and considering a blind volume, Couzin *et al.* [34] proposed a self-organizing model of group formation in 3D space. With this model, different collective behaviors of swarm, torus (milling), and parallel group (schooling) were exhibited [34,35]. Similar phase transition behaviors have also been identified in 2D space [10,12,36]. Although some researchers have done a lot of research on 3D collective behaviors, most of them depend on the metric interaction or the n closest neighbors [18,29,37,38], which cannot fully cover the observations in nature, such as "bait ball" [13]. The

*Corresponding author: zjudengjian@zju.edu.cn

understanding of collective motions in 3D space is still not adequate.

In this study, we propose a 3D model of collective behavior based on the PTW model by considering the first shell of a Voronoi tessellation as the neighbors. While it was stated that the interacting neighbors determined by the Voronoi tessellation (approximately 15 in three dimensions) cannot be tuned in Ref. [25], we disagree with that statement. Actually, by introducing a continuously varied rear blind angle, our model simulates with five to eight neighbors, consistently in line with the previous observations [23–25]. By varying the alignment and noise intensities, we draw a comprehensive map in their space, with different patterns of collective motions identified. More importantly, we quantify the tridimensionality, which is not available in the previous 2D studies.

II. NUMERICAL METHODOLOGY

If we characterize each individual by its position $\mathbf{r}_i$ and velocity $\dot{\mathbf{r}}_i$, the dynamical equations of motion can be simply written as

$$\mathbf{r}_i = [x_i, y_i, z_i]^{\mathbf{T}} \tag{1}$$

and

$$\mathbf{r}_{i,t+1} = \mathbf{r}_{i,t} + \Delta t \cdot \dot{\mathbf{r}}_{i,t}. \tag{2}$$

We assume that each individual moves with a constant unit speed along its orientation $\mathbf{e}_i^{\parallel}$, which is written as

$$\dot{\mathbf{r}}_i = \mathbf{e}_i^{\parallel} = [e_{i,x}^{\parallel}, e_{i,y}^{\parallel}, e_{i,z}^{\parallel}]^{\mathbf{T}}. \tag{3}$$

It is updated by

$$\mathbf{e}_{i,t+1}^{\parallel} = \frac{\mathcal{R}_x\mathcal{R}_y\mathcal{R}_z\mathbf{e}_{i,t}^{\parallel} + \sum_{j\in V_i}\mathbf{f}_{ij}}{\left|\mathcal{R}_x\mathcal{R}_y\mathcal{R}_z\mathbf{e}_{i,t}^{\parallel} + \sum_{j\in V_i}\mathbf{f}_{ij}\right|}, \tag{4}$$

where $\mathcal{R}_x$, $\mathcal{R}_y$, and $\mathcal{R}_z$ are the rotation matrices with respect to the three coordinate axes, and $\mathbf{f}_{ij}$ is the repulsive force avoiding collisions. The rotation matrices are defined as

$$\mathcal{R}_x = \begin{bmatrix} 1 & 0 & 0 \\ 0 & \cos(\omega_x\Delta t) & -\sin(\omega_x\Delta t) \\ 0 & \sin(\omega_x\Delta t) & \cos(\omega_x\Delta t) \end{bmatrix}, \tag{5}$$

$$\mathcal{R}_y = \begin{bmatrix} \cos(\omega_y\Delta t) & 0 & \sin(\omega_y\Delta t) \\ 0 & 1 & 0 \\ -\sin(\omega_y\Delta t) & 0 & \cos(\omega_y\Delta t) \end{bmatrix}, \tag{6}$$

$$\mathcal{R}_z = \begin{bmatrix} \cos(\omega_z\Delta t) & -\sin(\omega_z\Delta t) & 0 \\ \sin(\omega_z\Delta t) & \cos(\omega_z\Delta t) & 0 \\ 0 & 0 & 1 \end{bmatrix}, \tag{7}$$

where a visual representation of the rotations involved can be seen in Fig. 1, in which the angular velocity $\boldsymbol{\omega}$ can be described as the sum of an attraction term, an alignment term, and a noise, expressed as

$$[\omega_x, \omega_y, \omega_z]_i^{\mathbf{T}} = \langle \boldsymbol{\rho}_{ij} \times \mathbf{e}_i^{\parallel} + I_{\parallel}\mathbf{e}_i^{\parallel} \times \mathbf{e}_j^{\parallel} \rangle + I_n\boldsymbol{\eta}. \tag{8}$$

Here, $\boldsymbol{\rho}_{ij}$ is a distance vector pointing from an individual i to its neighbor j, $I_{\parallel}$ is the alignment intensity, I_n is the noise intensity, and $\boldsymbol{\eta}$ is a random unit vector generated by a

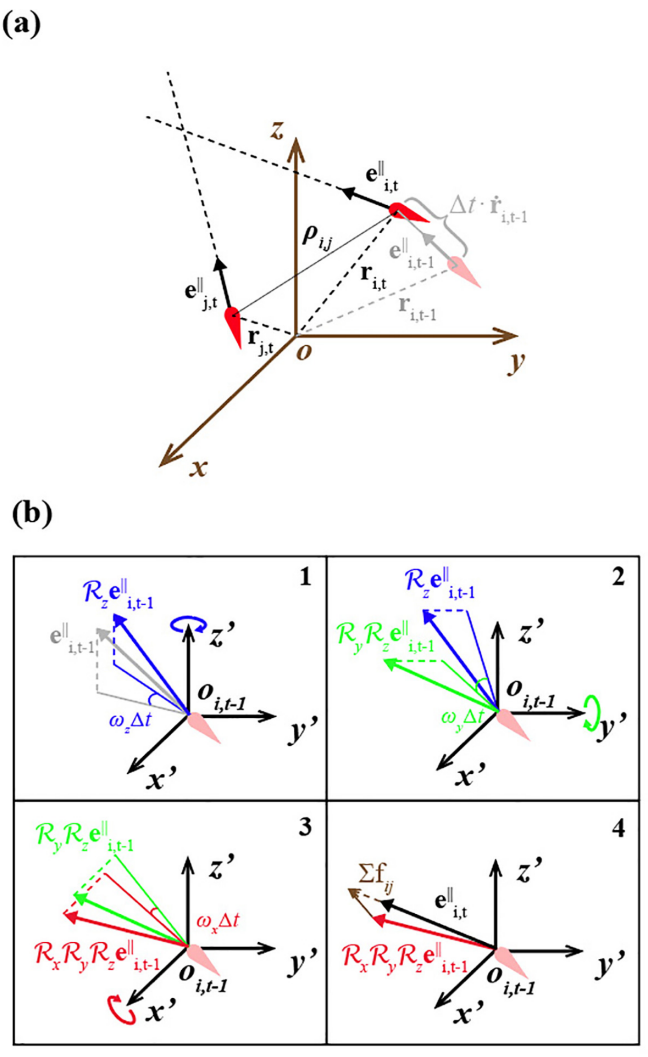

FIG. 1. (a) Sketch of two interacting individuals (red), showing the position $\mathbf{r}_i$ and $\mathbf{r}_j$, the orientation $\mathbf{e}_i^{\parallel}$ and $\mathbf{e}_j^{\parallel}$, the distance vector $\boldsymbol{\rho}_{ij}$ pointing from individual i to its neighbor j, and the moving vector for individual i from $t-1$ (pink) to t (red). (b) Substep sketch of Eq.(4), namely the rotation matrix and the repulsive force.

standard Wiener process, describing the spontaneous motion of the individual, and modeling its "free will". The attraction and alignment terms [the first and second products at the right side of Eq.(8)] are averaged over the Voronoi neighbors, noted V_i, with a weight, $(1+\zeta)$, representing the individual's anisotropic perception of its environment, denoted by

$$\langle \circ \rangle = \sum_{j\in V_i} \circ(1+\zeta) \Big/ \sum_{j\in V_i}(1+\zeta), \tag{9}$$

with

$$\zeta = \mathbf{e}_i^{\parallel} \cdot \frac{\boldsymbol{\rho}_{ij}}{|\rho_{ij}|}. \tag{10}$$

We note that $(1+\zeta)$ models continuously a rear blind angle [10,12], which means that the individual does not get information from neighbors falling in its blind zone. Following the previous study [15], we introduce a short-range repulsive

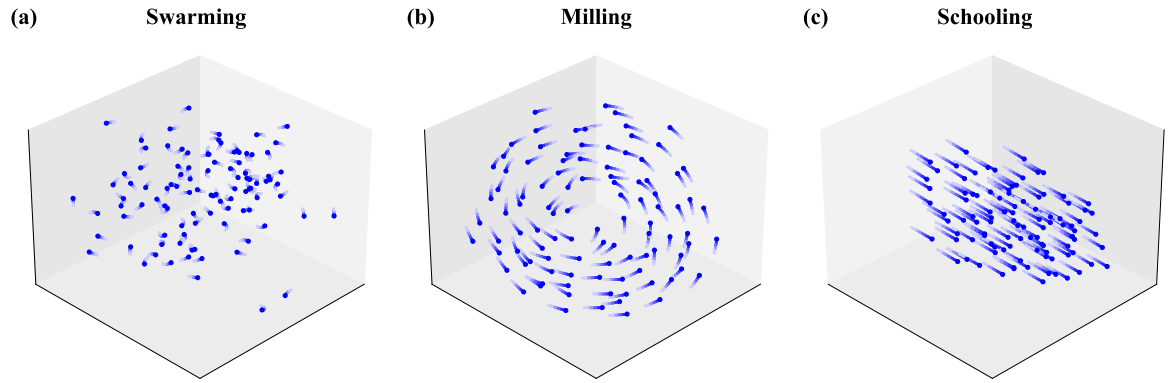

FIG. 2. The collective patterns exhibited by the model, with the snapshots of spatial individual distributions for (a) swarming at $I_{||} = 0.2$ and $I_n = 1.8$, (b) milling at $I_{||} = 0.6$ and $I_n = 0.2$, and (c) schooling at $I_{||} = 2.5$ and $I_n = 0.5$. For all simulations, $\beta = 1.0$, and the snapshots are taken at the end of 10 000 time units. Note that the data from five sequential time instants are superposed to represent the moving directions. For long-time dynamics, i.e., their evolution from randomly initialized positions and orientations in a $20 \times 20 \times 20$ cubic box, see movies 1–3 provided in the Supplemental Material [39].

interaction exerted by the individual's neighbors:

$$\mathbf{f}_{ij} = -\beta \frac{\boldsymbol{\rho}_{ij}}{|\boldsymbol{\rho}_{ij}|\left(1 + e^{\left(\frac{|\boldsymbol{\rho}_{ij}|}{r_c} - 2\right)}\right)}, \tag{11}$$

where β measures the relative strength of repulsion with respect to alignment and noise strength. As reported in the previous study, the repulsive term is not necessary in a topology based model [12]. Here, we set $\beta = 1.0$ and $r_c = 0.072$ only to avoid the failure of Voronoi tessellation when $I_n = 0$, as then the school would perfectly align itself into a line. We should point out that the group is simulated in an open space, therefore there is no boundary condition involved.

III. RESULTS

We consider a group with 100 individuals. They are randomly distributed in a $20 \times 20 \times 20$ cubic box (in dimensionless length units). This dynamic system is solved numerically using an explicit scheme with time step $\Delta t = 10^{-2}$. Evolving after a few dimensionless time units, the group reaches a statistically steady state, exhibiting a discernible locomotive pattern. Here, depending on the values of alignment intensity $I_{||}$ and noise intensity I_n, three different patterns can be identified. They are "swarming", as shown in Fig. 2(a), exhibiting a disordered sparse group without preferential orientation; "schooling", as shown in Fig. 2(c), exhibiting a highly coordinated collective motion; and "milling", as shown in Fig. 2(b), which forms a "vortex" with each individual following an approximately circular trajectory. We refer the reader to the videos provided in the Supplemental Material [39] which clearly illustrate the emergence of different (collective) patterns from randomly initialized distributions.

The three different locomotive patterns can be characterized more precisely by two global order parameters P and M defined as

$$P = \frac{1}{N}\left|\sum_{i=1}^{N} \mathbf{e}_i^{\parallel}\right|, \quad M = N\frac{\left|\sum_{i=1}^{N} \mathbf{e}_i^{r} \times \dot{\mathbf{r}}_i\right|}{\left|\sum_{i=1}^{N} \mathbf{e}_i^{r}\right|\left|\sum_{i=1}^{N} \dot{\mathbf{r}}_i\right|}, \tag{12}$$

where N is the number of individuals, $\mathbf{e}_i^r$ is the unit vector directed along the segment going from the mass center of the

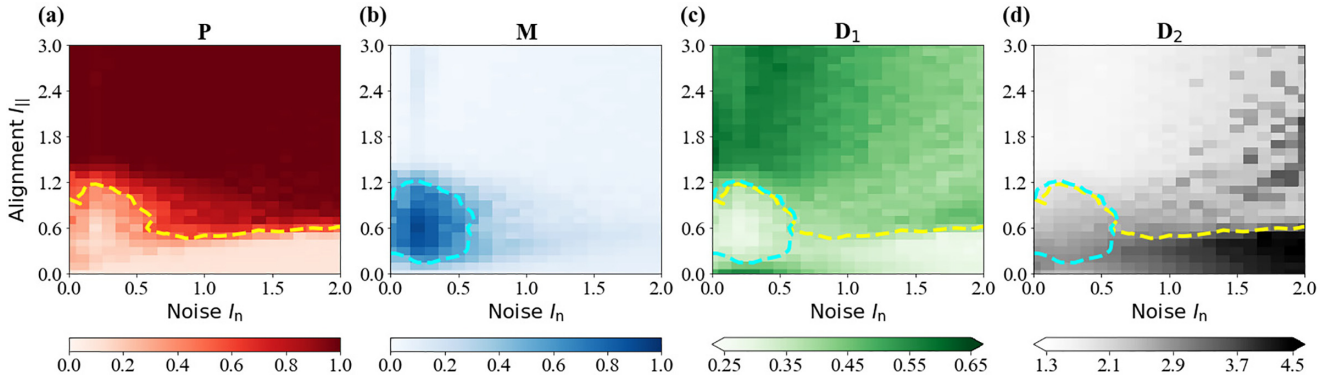

FIG. 3. Contour plots of P, M, D_1, and D_2 in the $(I_n, I_{||})$ parametric space: (a) the polarization P with the dashed yellow line of $P = 0.5$ marking the phase transition to a highly coordinated schooling pattern as $I_{||}$ is high; (b) the milling M identifying a milling pattern at the bottom left corner from the rest regimes, with $M = 0.5$ (the dashed cyan line); (c) the dimension indicator D_1 gives a value of 0.1 for a planar spatial structure, while 1.0 for a sphere, and here, the superposition of the lines for $P = 0.5$ and $M = 0.5$ separates the swarming pattern to the bottom right of the space; (d) the distance D_2 indicates the spatial distance of the group (the average distance from individuals to the group center). A hundred simulations are run for each pair of I_n and $I_{||}$ with 10 000 time units, and the last 1000 time units are taken out for averaging.

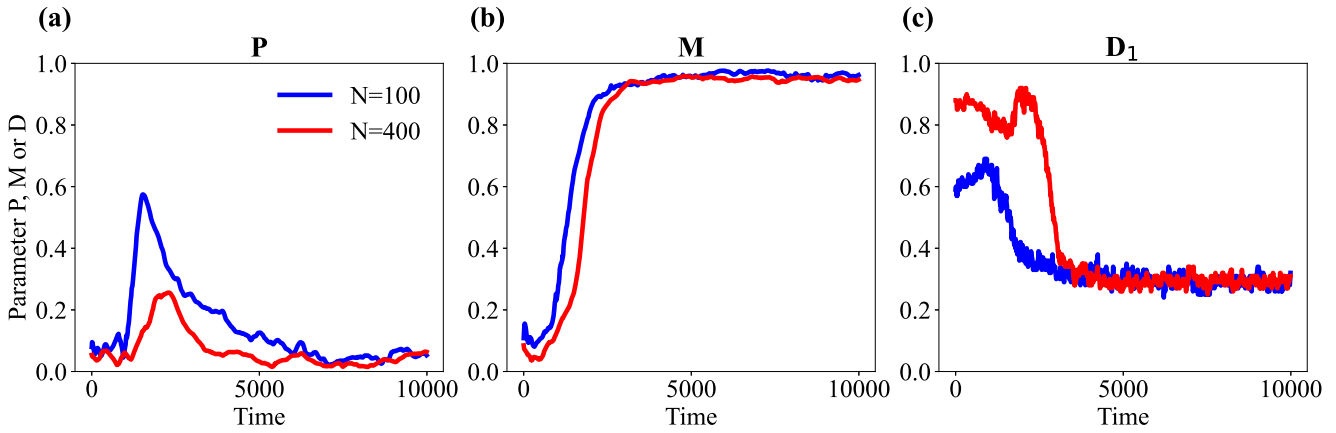

FIG. 4. Time histories of P, M, and D_1 at $(I_n, I_{||})$=(0.0,0.7), corresponding to a milling pattern, with two different individual numbers of $N = 100$ (blue lines) and $N = 400$ (red lines), while keeping group density the same. It demonstrates the independence of individual number in this topological neighborhood based model.

group to the ith individual. Moreover, we introduce another two parameters D_1 and D_2 to characterize, respectively, its threedimensionality and compactness. D_1 is calculated by projecting normally to a unit sphere centered at the mass center of the group, with its value representing a ratio between a summation of projected area and the sphere's area. It is easy to understand that when the individuals are distributed uniformly in the space, D_1 tends to be unity, therefore its value varies between zero and one. D_2 is an averaged distance from each individual to the mass center of the group, which can measure the scale of the group. In Fig. 3 we now proceed to investigate the the $(I_n, I_{||})$ parametric space. Here, the schooling and milling patterns can be easily distinguished from swarming by examining P and M, The group exhibits a disordered swarming pattern when noise dominates over the alignment rule, which emerges at the bottom right region of the parametric space [see Fig. 3(c)], where both P and M are small. At the bottom left corner of the parametric space, when the alignment and noise are comparable, the group involves into a milling pattern. When the alignment is strong compared to the noise, the group members tend to move in the same directions, which is known as the highly coordinated schooling

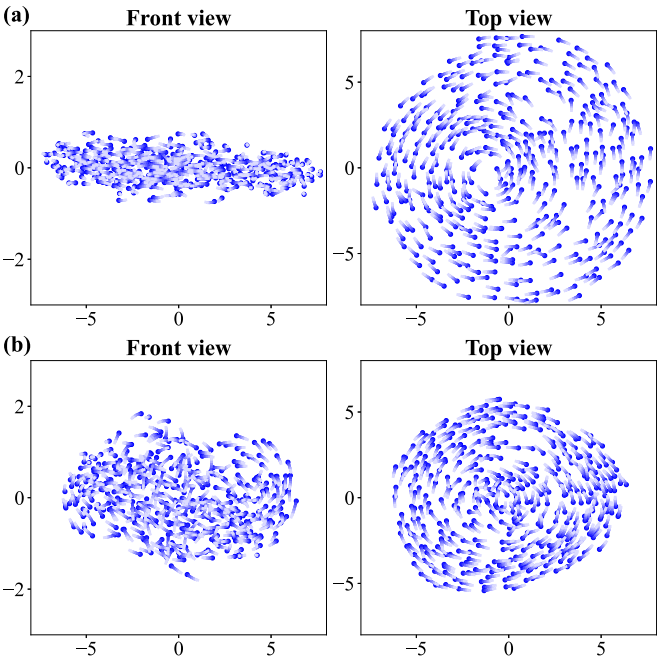

FIG. 5. Snapshots of two distinct milling patterns simulated with 400 individuals: (a) a flat milling structure at $(I_n, I_{||})$=(0.2, 0.6), with $D_1 = 0.283$ and $D_2 = 5.02$; (b) a bait ball at $(I_n, I_{||})$=(0.2, 0.9), with $D_1 = 0.585$ and $D_2 = 4.01$. Here, the snapshots are taken at the end of simulations, and D_1 and D_2 are averaged over the last 1000 time steps. Note that the views are adjusted according to their rotating axes for clearer presentation and more appropriate comparison. Please see movies four and five provided in the Supplemental Material [39] for the long-time dynamics of (a) and (b) respectively.

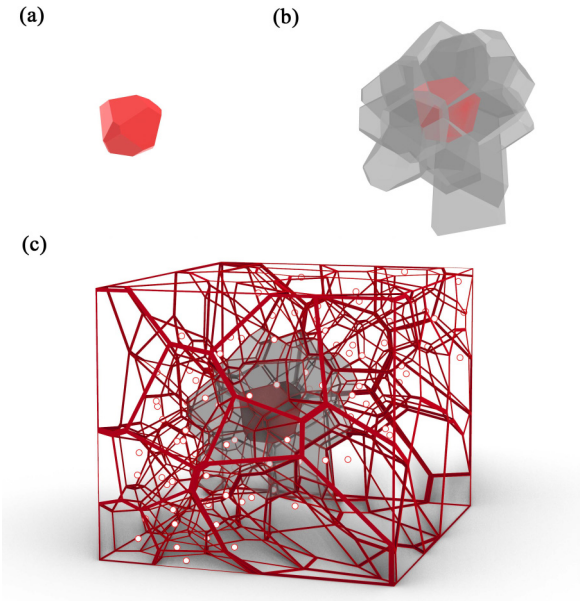

FIG. 6. Sketch of 3D Voronoi neighbors for a schooling pattern, where (a) the red cell represents the focal individual, (b) the transparent gray cells represent its first shell of Voronoi neighbors, and (c) voronoi tessellation for the entire group.

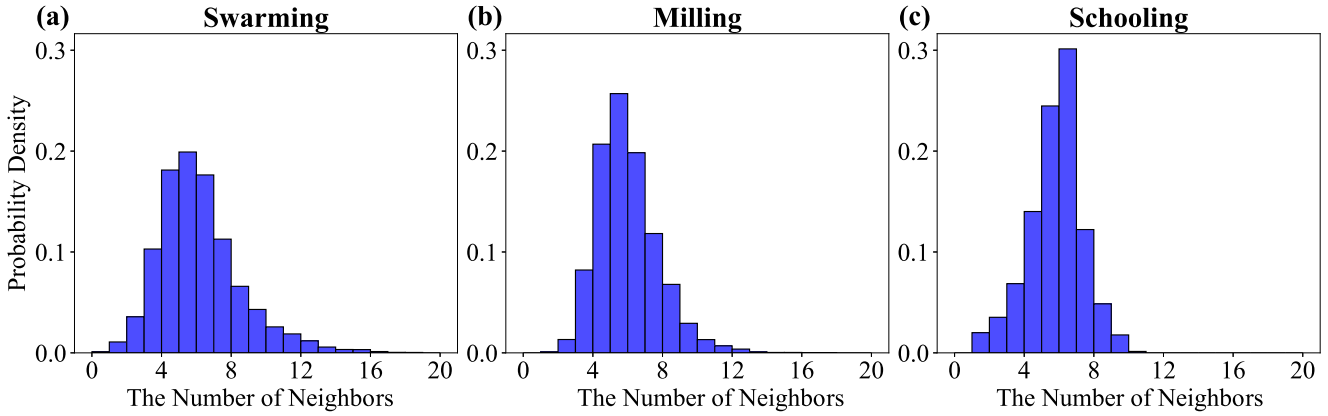

FIG. 7. The probability density of the average number of neighbors for different values of the parameters: (a) swarming for $(I_n, I_{||}) = (1, 8, 0.2)$; (b) milling for $(I_n, I_{||}) = (0.2, 0.6)$; and (c) schooling for $(I_n, I_{||}) = (0.5, 2.5)$. Each histogram is the result of an average over 100 different simulations in the same set of parameters.

pattern. These patterns are consistent with the previous study confined in a 2D space [12]. The schooling pattern presents a three-dimensional uniformality according to D_1, as shown in Fig. 3(c), and more compact spatial distributions, seen from Fig. 3(d). We note that in the current topological model the number of individuals does not change the statistically steady state much if we keep the group density the same. We demonstrate this property by choosing a specific case and monitoring the variations of P, M, and D_1 with time, as shown in Fig. 4. Clearly, the systems with individual numbers of $N = 100$ and $N = 400$ show the same long-time behavior as when the group density is fixed at 0.0125 per unit volume.

As observed in open water, a bait ball, or baitball, occurs when small fish swarm in a tightly packed spherical formation about a common center, which is believed to be a defensive measure adopted by small schooling fish when they are threatened by predators [40]. In 3D space, we observe two different modes of this behavior, as shown in Fig. 5. At the center of the milling pattern region according to Fig. 3, the group resembles that of the 2D space, forming a flat milling structure, in which the individuals move vortically around an central axis, though which is a time varying vector. In contrast, near the boundary of this milling region, the group tends to form a more spherical ball, when a rotating axis cannot be identified. In Fig. 5, at this specific instant, the flat, milling structure and the more tridimensional, balling structure can also be distinguished by D_1. Clearly, the balling structure has a larger value of D_1. Also it has a more compact spatial structure, or a smaller D_2, comparing to the flat, milling structure.

In Fig. 6, we choose a specific case with a schooling pattern to present the three-dimensional topology of the group structure. For clarity, we enclose the simulated group with a cubic box. We show a specific Voronoi cell [see Fig. 6(a)] and its neighboring cells [the first shell of Voronoi tessellation, see Fig. 6(b)]. The cell shown in Fig. 6(a) is a polyhedron with 15 facets. However, as we consider the blind angle, represented by Eq. (9), the number of neighbors an individual actually interacts with is around 4–8, which varies among different patterns. As shown in Fig. 7, the individual in a milling group interacts most likely with 5–6 neighbors, while that in a schooling group interacts with 6–7 neighbors, falling exactly in the range of field observations for starling flocks (7 ± 1.5 closest neighbors [23–25]).

IV. CONCLUSIONS

In summary, we propose a 3D numerical model for collective motion, which can reduplicate the collective patterns observed in the previous 2D studies, such as swarming, milling, and schooling, and beyond that a more realistic bait ball can be observed, differentiating from the flat, two-dimensional milling structure. More significantly, this model is well consistent with the field observations in terms of the neighboring number an individual can interact with.

Future extension of the present work might be devoted to the variations of group density. Intuitively, the system with a higher density tends to form a more compact structure, particularly for the balling pattern. Please see movies six and seven provided in the Supplemental Material [39] simulated, respectively, at $(I_n, I_{||})$=(0.0, 0.9) and (0.2, 1.3) with a higher density of 0.05 per unit volume.

ACKNOWLEDGMENTS

This research has been supported by the National Natural Science Foundation of China (Grants No. 92252102 and No. 11922212).

[1] A. Deutsch, G. Theraulaz, and T. Vicsek, Collective motion in biological systems, Interface Focus **2**, 689 (2012).

[2] O. Feinerman, I. Pinkoviezky, A. Gelblum, E. Fonio, and N. S. Gov, The physics of cooperative transport in groups of ants, Nat. Phys. **14**, 683 (2018).

[3] D. Mateo, N. Horsevad, V. Hassani, M. Chamanbaz, and R. Bouffanais, Optimal network topology for responsive collective behavior, Sci. Adv. **5**, eaau0999 (2019).

[4] D. Martin, H. Chaté, C. Nardini, A. Solon, J. Tailleur, and F. Van Wijland, Fluctuation-Induced Phase Separation in Metric

and Topological Models of Collective Motion, Phys. Rev. Lett. **126**, 148001 (2021).
[5] T. Vicsek, A. Czirók, E. Ben-Jacob, I. Cohen, and O. Shochet, Novel Type of Phase Transition in a System of Self-Driven Particles, Phys. Rev. Lett. **75**, 1226 (1995).
[6] T. Vicsek and A. Zafeiris, Collective motion, Phys. Rep. **517**, 71 (2012).
[7] F. Ginelli, The physics of the vicsek model, Eur. Phys. J.: Spec. Top. **225**, 2099 (2016).
[8] J. Gautrais, C. Jost, M. Soria, A. Campo, S. Motsch, R. Fournier, S. Blanco, and G. Theraulaz, Analyzing fish movement as a persistent turning walker, J. Math. Biol. **58**, 429 (2009).
[9] J. Gautrais, F. Ginelli, R. Fournier, S. Blanco, M. Soria, H. Chaté, and G. Theraulaz, Deciphering interactions in moving animal groups, PLoS Comput Biol **8**, e1002678 (2012).
[10] D. S. Calovi, U. Lopez, S. Ngo, C. Sire, H. Chaté, and G. Theraulaz, Swarming, schooling, milling: phase diagram of a data-driven fish school model, New J. Phys. **16**, 015026 (2014).
[11] D. S. Calovi, U. Lopez, P. Schuhmacher, H. Chaté, C. Sire, and G. Theraulaz, Collective response to perturbations in a data-driven fish school model, J. R. Soc. Interface. **12**, 20141362 (2015).
[12] A. Filella, F. Nadal, C. Sire, E. Kanso, and C. Eloy, Model of Collective Fish Behavior with Hydrodynamic Interactions, Phys. Rev. Lett. **120**, 198101 (2018).
[13] U. Lopez, J. Gautrais, I. D. Couzin, and G. Theraulaz, From behavioural analyses to models of collective motion in fish schools, Interface Focus **2**, 693 (2012).
[14] G. Grégoire, H. Chaté, and Y. Tu, Moving and staying together without a leader, Physica D **181**, 157 (2003).
[15] H. Chaté, F. Ginelli, G. Grégoire, and F. Raynaud, Collective motion of self-propelled particles interacting without cohesion, Phys. Rev. E **77**, 046113 (2008).
[16] P. De Lellis and M. Porfiri, Inferring the size of a collective of self-propelled vicsek particles from the random motion of a single unit, Commun. Phys. **5**, 86 (2022).
[17] M. Zumaya, H. Larralde, and M. Aldana, Delay in the dispersal of flocks moving in unbounded space using long-range interactions, Sci. Rep. **8**, 15872 (2018).
[18] R. K. Mudaliar, A. V. Zvezdin, G. S. Bratt, and T. M. Schaerf, Systematic analysis of emergent collective motion produced by a 3d hybrid zonal model, Bull. Math. Biol. **84**, 16 (2022).
[19] F. Ginelli and H. Chaté, Relevance of Metric-Free Interactions in Flocking Phenomena, Phys. Rev. Lett. **105**, 168103 (2010).
[20] A. Strandburg-Peshkin, C. R. Twomey, N. W. Bode, A. B. Kao, Y. Katz, C. C. Ioannou, S. B. Rosenthal, C. J. Torney, H. S. Wu, S. A. Levin *et al.*, Visual sensory networks and effective information transfer in animal groups, Curr. Biol. **23**, R709 (2013).
[21] R. Bastien and P. Romanczuk, A model of collective behavior based purely on vision, Sci. Adv. **6**, eaay0792 (2020).
[22] S. Roy and J. Lemus, How does the fusion of sensory information from audition and vision impact collective behavior? Front. Appl. Math. Stat. **7**, 758711 (2021).
[23] A. Cavagna, A. Cimarelli, I. Giardina, G. Parisi, R. Santagati, F. Stefanini, and R. Tavarone, From empirical data to inter-individual interactions: Unveiling the rules of collective animal behavior, Math. Models Methods Appl. Sci. **20**, 1491 (2010).
[24] M. Ballerini, N. Cabibbo, R. Candelier, A. Cavagna, E. Cisbani, I. Giardina, V. Lecomte, A. Orlandi, G. Parisi, A. Procaccini *et al.*, Interaction ruling animal collective behavior depends on topological rather than metric distance: Evidence from a field study, Proc. Natl. Acad. Sci. **105**, 1232 (2008).
[25] M. Camperi, A. Cavagna, I. Giardina, G. Parisi, and E. Silvestri, Spatially balanced topological interaction grants optimal cohesion in flocking models, Interface Focus **2**, 715 (2012).
[26] R. Escobedo, V. Lecheval, V. Papaspyros, F. Bonnet, F. Mondada, C. Sire, and G. Theraulaz, A data-driven method for reconstructing and modelling social interactions in moving animal groups, Philos. Trans. R. Soc. B **375**, 20190380 (2020).
[27] H. Ling, G. E. Mclvor, J. Westley, K. van der Vaart, R. T. Vaughan, A. Thornton, and N. T. Ouellette, Behavioural plasticity and the transition to order in jackdaw flocks, Nat. Commun. **10**, 5174 (2019).
[28] L. Lei, R. Escobedo, C. Sire, and G. Theraulaz, Computational and robotic modeling reveal parsimonious combinations of interactions between individuals in schooling fish, PLoS Comput. Biol. **16**, e1007194 (2020).
[29] A. Czirók, M. Vicsek, and T. Vicsek, Collective motion of organisms in three dimensions, Physica A **264**, 299 (1999).
[30] B. Gönci, M. Nagy, and T. Vicsek, Phase transition in the scalar noise model of collective motion in three dimensions, Eur. Phys. J.: Spec. Top. **157**, 53 (2008).
[31] P. Szabó, M. Nagy, and T. Vicsek, Transitions in a self-propelled-particles model with coupling of accelerations, Phys. Rev. E **79**, 021908 (2009).
[32] M. L. Rubio Puzzo, A. De Virgiliis, and T. S. Grigera, Self-propelled vicsek particles at low speed and low density, Phys. Rev. E **99**, 052602 (2019).
[33] Y. Wu, J. Li, D. Chen, X. Li, and H.-T. Zhang, Pattern phase transitions in 3d minimal vicsek model, Europhys. Lett. **134**, 50004 (2021).
[34] I. D. Couzin, J. Krause, R. James, G. D. Ruxton, and N. R. Franks, Collective memory and spatial sorting in animal groups, J. Theor. Biol. **218**, 1 (2002).
[35] H. Koorehdavoudi and P. Bogdan, A statistical physics characterization of the complex systems dynamics: Quantifying complexity from spatio-temporal interactions, Sci. Rep. **6**, 27602 (2016).
[36] J. Deng and D. Liu, Spontaneous response of a self-organized fish school to a predator, Bioinspiration & Biomimetics **16**, 046013 (2021).
[37] C. W. Reynolds, Flocks, herds and schools: A distributed behavioral model, Computer Graphics **21**, 25 (1987).
[38] Q. Li, L. Zhang, Y. Jia, T. Lu, and X. Chen, Modeling, analysis, and optimization of three-dimensional restricted visual field metric-free swarms, Chaos, Solitons Fractals **157**, 111879 (2022).
[39] See Supplemental Material at http://link.aps.org/supplemental/10.1103/PhysRevE.107.014606 for videos illustrating the long-time dynamics shown in Figs. 2 and 5.
[40] B. L. Partridge, The structure and function of fish schools, Sci. Am. **246**, 114 (1982).